AIAA JOURNAL
Vol. 34, No. 2, February 1996

Investigation of High-Order Upwinded Differencing for Vortex Convection

Brian E. Wake* and Dochul Choi†
United Technologies Research Center, East Hartford, Connecticut 06108

Two model problems were formulated to investigate the benefits of using higher order upwinded differencing schemes to convect a vortex. In these model problems, one or two ideal vortices were specified at the upstream boundary and convected through a simple fluid domain in the direction of the vorticity vector. Numerical tests were performed using an implicit upwinded finite volume method with orders of accuracy varying from first to fifth order. The effect of grid refinement was examined to determine the relative advantage to higher order accuracy vs additional grid points. The calculations demonstrated that the fifth-order scheme with 14 points across the vortex diameter convected a well-aligned vortex almost perfectly. The fifth-order scheme provided a factor of 10 reduction in the number of points over the third-order scheme in each crossflow plane. The corotating double-vortex model problem was used to study the effect of vortex skewness relative to the grid. A vortex-convection skewness parameter was defined that indicates the number of grid points required in the axial direction for adequate preservation of a vortex skewed relative to the grid. Although the higher order schemes improved the results considerably, it was found that the axial grid spacing was limited even for small vortex skew angles relative to the grid.

Nomenclature

A_R = grid cell aspect ratio, $\Delta x/\Delta r$
a_l = coefficients for the damping function
c = chord length, 10
D = damping function
F = inviscid flux vector
n_v = number of grid points across the vortex diameter
Q = vector of conserved flow quantities
Re = Reynolds number, $\rho c u_v/\mu$
r = radial coordinate centered at vortex center, $r^2 = (y - y_c)^2 + (z - z_c)^2$
r_v = vortex core radius
S = matrix of eigenvectors
u_{cv} = crossflow magnitude of vortex convection velocity, $(v_v^2 + w_v^2)^{1/2}$
u_v = axial convection velocity of vortex
u_θ = tangential velocity (θ direction)
u, v, w = Cartesian components of velocity
v_v, w_v = y and z components of the vortex convection velocity
x = axial coordinate
y, z = crossflow Cartesian coordinates
y_c, z_c = vortex center
α_l = coefficient of finite difference stencil
β = constant used in stencil
γ = constant used in truncation term
Δr = grid spacing in radial direction, $\Delta y \sin\theta + \Delta z \cos\theta$
Δv = peak-to-peak velocity across vortex
Δv_0 = initial value of Δv, $x = 0$
Δx = axial grid spacing
$\Delta y, \Delta z$ = crossflow Cartesian grid spacing
η_v = vortex-convection skewness parameter, $u_{cv}\Delta x/u_v\Delta r = A_R \tan\varphi_v$
θ = tangential coordinate relative to vortex center, $\tan^{-1}[(y - y_c)/(z - z_c)]$
Λ = vector of eigenvalues
μ = molecular viscosity
ρ = fluid density
φ_v = angle between axial grid and vortex path, $\tan^{-1}(u_{cv}/u_v)$
ω = magnitude of vorticity

Received May 5, 1995; presented as Paper 95-1719 at the AIAA 12th Computational Fluid Dynamics Conference, San Diego, CA, June 19–22, 1995; revision received Sept. 12, 1995; accepted for publication Sept. 18, 1995.

*Research Engineer, Physical and Mathematical Modeling, 411 Main Street. Member AIAA.
†Senior Research Engineer, Physical and Mathematical Modeling, 411 Main Street. Member AIAA.

Introduction

WITH the increased performance of workstations and supercomputers, three-dimensional Navier–Stokes solvers are being used by industry today for a myriad of applications. Navier–Stokes solvers have proven useful for the examination of detailed and gross flow features, as well as engineering design. One of primary deficiencies of current Euler and Navier–Stokes solvers is their inability to adequately convect vorticity. The vorticity predicted by numerical methods diffuses too rapidly due to the inherent numerical dissipation of the scheme. For some applications, the usefulness of Navier–Stokes solvers is severely limited by this shortcoming. Accurate resolution of vorticity is important for many practical problems, including rotary- and fixed-wing aerodynamics, turbomachinery, vortex generators, and configurations with flow separation. Using an increasingly finer grid is not a practical solution for many problems of interest.

Predicting the performance of a helicopter rotor is one example of the problem presented by numerical diffusion. In hover, the helicopter rotor blade sheds a strong tip vortex that maintains its structure for several rotor revolutions. The helical tip vortex induces a strong rotor downwash that cannot be neglected. For an accurate prediction of the hovering performance, this tip vortex must be captured accurately, especially for the first blade passage (one-fourth of a revolution for a four-bladed rotor). A schematic of this is shown in Fig. 1. The local induced velocity due to this passing vortex has a significant effect on the blade loads and the resulting performance of the rotor. In forward flight, the problem is even more difficult since the vortex geometry is very complex and arbitrary relative to the grid.

The velocity profile of the tip vortex represents a near discontinuity in the flowfield relative to the grid resolution generally used. The peak-to-peak velocities across the vortex core are typically of the same order as the freestream velocity. The vortex core radius r_v is nominally one-tenth of the tip chord length. To reach the next rotor blade of a four-bladed rotor, the tip vortex must be convected over

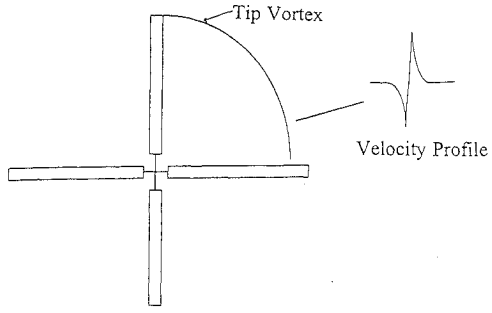

Fig. 1 Schematic diagram depicting tip vortex of a helicopter rotor in hover.

a distance of about $250r_v$ without noticeable diffusion. For many problems, the vortex trajectory will be skewed relative to the grid. When the vortex trajectory is complex, its orientation is arbitrary relative to the grid. For this case, there will be essentially no distinction between the crossflow grid spacing and the axial grid spacing. The number of grid points required to resolve the vortex will scale with n_v^3 instead of n_v^2.

There are several examples of previous work in this area. Calculations for hover using the TURNS analysis[1,2] demonstrated that the vortex is severely diffused by the first blade passage when using 900,000 grid points. Much of the problem was due to an inadequate placement of grid points. This is being addressed by multiblock[3] and unstructured flow solvers.[4] Another potential source for improvement is to increase the order of accuracy. Calculations have been performed previously by others using fifth-order accurate differencing to resolve the helicopter tip vortex in hover[5] and a fixed-wing tip vortex.[6] Fifth-order accuracy improved the resolution significantly over the third-order methods, but relative to experiment, the calculations still require much improvement.

The objectives of the study described in this paper were to determine how well the vortex could be maintained using standard low-order upwinded methods (first and second order), given a reasonable number of grid points within the vortex core, to assess the advantages of higher order schemes (third and fifth order) vs grid refinement, and to examine the importance of axial grid spacing and grid aspect ratio for the convection of a vortex skewed relative to the grid. Studying the effect of these parameters and assessing the benefit of higher order methods are difficult for a large problem such as the wing. To address these issues, two model problems were formulated to study the fundamental problem of convecting a tip vortex.

Numerical Method

The Navier–Stokes analysis used in this study was the upwinding-based time-dependent Navier–Stokes (UTNS) code. This analysis solves the compressible Navier–Stokes equations with a two-equation q–ω turbulence model. The numerical scheme is a cell-based finite volume technique and uses upwind-biased differencing. The details of the numerical scheme developed before this study can be found in Refs. 7–10. Some of the specific features of the scheme used in UTNS code are described here.

The accuracy of the convective terms varies from first to fifth order. The various orders of accuracy are achieved by interpolation of the characteristic variables to the cell faces. The interpolation stencils are derived by a Taylor series expansion about the half-points. Upwind-biased numerical stencils are used for the third- and fifth-order accurate schemes to limit the stencil lengths of the first derivatives to $n+1$ points for an nth-order scheme. The first- and second-order stencils are fully upwinded. Note that these higher order schemes are only formally nth order accurate for the one-dimensional linear problem.

The ξ-directional inviscid convection term is expressed in a finite difference form as

$$\frac{\partial F_i}{\partial \xi} = \frac{\tilde{F}_{i+\frac{1}{2}} - \tilde{F}_{i-\frac{1}{2}}}{\Delta \xi} \tag{1}$$

Table 1 Stencil coefficients and leading truncation term for nth-order evaluation of $\partial F/\partial \xi$

n	α_{i-3}	α_{i-2}	α_{i-1}	α_i	α_{i+1}	α_{i+2}	β	γ
1	——	——	−1	1	——	——	1	−2
2	——	1	−4	3	——	——	2	−3
3	——	1	−6	3	2	——	6	12
5	−2	15	−60	20	30	−3	60	−60

where $\tilde{F}_{i+1/2} = \frac{1}{2}(F_{i+1} + F_i - D_{i+1/2})$, and the damping function D has the form

$$D_{i+\frac{1}{2}} = S^{-1} \cdot |\Lambda| \cdot \sum_l a_l (S \cdot \delta Q)_l$$
$$\delta Q_l = Q_{l+1} - Q_l \tag{2}$$

The signs of the eigenvalues determine the correct biasing direction to use for each characteristic variable at each face. The $S^{-1} \cdot |\Lambda|$ terms are calculated at the $i+\frac{1}{2}$ location, whereas the $S \cdot \delta Q$ term is computed over a range of cell-face locations that depends on the order of accuracy. The coefficients a_l in the summation of the damping function and the range of the cell-face locations l are defined such that the desired accuracy of the first derivative is obtained. Flux limiters were not used for these applications.

The equivalent nth-order finite difference stencils for the first derivative of the flux have the form

$$\frac{\partial F_i}{\partial \xi} = \frac{1}{\beta \Delta \xi} \sum_{l=i-3}^{i+4} \alpha_l F_l + \frac{\Delta \xi^n}{\gamma} \frac{\partial^{n+1} F_i}{\partial \xi^{n+1}} + \cdots \tag{3}$$

The coefficients for this equation are given in Table 1. These stencils are biased in the decreasing i direction and are used for positive eigenvalues. For negative eigenvalues, the stencils are a mirror image about the i location, with a change of sign of the coefficients. The eigenvalues at the cell faces are calculated using Roe's averaging.[11]

For the implicit operator, a diagonalized alternating direction implicit scheme based on first-order upwinding is used with a fully implicit treatment of boundary conditions. This solver has been validated for a broad range of problems from incompressible flows to hypersonic flow regimes.[7–10] Note that most of the applications for practical engineering problems have been limited to second- or third-order accuracy with an optional total variation diminishing scheme.

Model Problems

In the discussions that follow, all lengths are normalized by r_v and velocities by u_v. The model problems examined in this study consist of one or two ideal tip vortices convected through a simple fluid domain in the axial direction. The single-vortex model problem is similar to the Euler and Helmholtz problems studied previously by others.[12–14] In Fig. 2, schematic diagrams of the single-vortex and double-vortex model problems are provided. The crossflow plane consists of the y and z coordinates, and the x coordinate is the axial direction. The corotating double-vortex model problem is an unique one that was studied to examine the effect of the vortex-convection skewness relative to the computational grid. For the single-vortex problem the convection of the vortex was perfectly aligned with the mesh. This eliminated much of the solution's dependence on axial grid spacing. For real problems, there will always be some skewness relative to the grid. The corotating vortices of the double-vortex model problem rotate about one another as they convect axially. This produces a constant vortex skew angle relative to the mesh without causing the vortices to leave the simple domain.

Two velocity profiles were studied for the single-vortex problem: the Rankine vortex and the Lamb–Oseen vortex. The Rankine and Lamb–Oseen vortex velocity profiles are shown in Fig. 3. The Rankine vortex is an idealized profile that assumes a linear variation of velocity with distance from the center r inside the core, and a $1/r$ variation outside the core. This vortex is not realistic since the derivatives of velocity (and hence vorticity) are not defined for $r = 1$. The Rankine vortex was more difficult to model because of its very sharp velocity peak and provided a very demanding test for the flow solver. A more realistic profile is that of Lamb and Oseen[15]

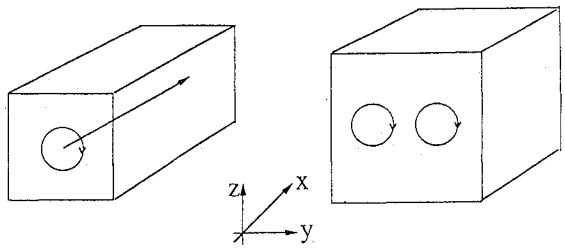

Fig. 2 Schematic diagrams of the single-vortex and double-vortex model problems.

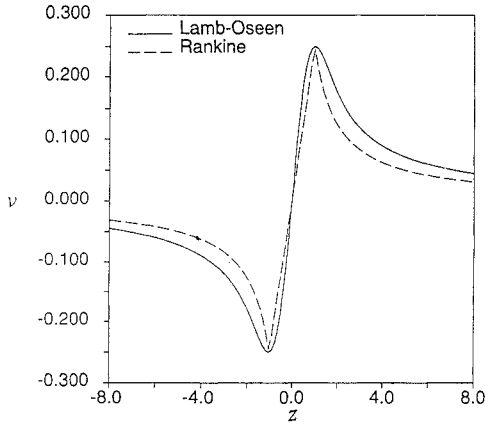

Fig. 3 Vertical velocity component across the center of the ideal Rankine and Lamb–Oseen vortices.

for which finite curvature exists at the peaks of the velocity profile. The emphasis was placed on the Lamb–Oseen vortex profile because it is more realistic.

Mathematical Formulation

The Lamb–Oseen vortex profile is a solution of the two-dimensional incompressible Navier–Stokes equations and is described by an exponential function. The equation for tangential velocity u_θ is

$$u_\theta = (0.7155/r)\Delta v\left(1 - e^{-1.2r^2}\right) \tag{4}$$

$$r^2 = [y - y_c(x)]^2 + [z - z_c(x)]^2 \tag{5}$$

The coordinates y_c and z_c represent the center of the vortex, which is a function of x for a skewed vortex and depends on the vortex-convection velocities, u_v, v_v, and w_v. Equation (4) is used to define the upstream velocity distribution of the three-dimensional domain.

To estimate the axial spacing required to produce an accuracy consistent with the crossflow spacing for a skewed vortex, the velocity gradient in the axial direction was computed by differentiating Eqs. (4) and (5):

$$\frac{\partial u_\theta}{\partial x} = \frac{\partial u_\theta}{\partial r}\left(\frac{\partial r}{\partial x}\right) = \frac{\partial u_\theta}{\partial r}\left(-\frac{\partial y_c}{\partial x}\sin\theta - \frac{\partial z_c}{\partial x}\cos\theta\right) \tag{6}$$

where $\partial y_c/\partial x = v_v/u_v$ and $\partial z_c/\partial x = w_v/u_v$. The axial gradient of u_θ is largest when $\partial r/\partial x$ is maximum. This occurs for a value of θ such that $\tan\theta = v_v/w_v$. It then follows that $\sin\theta = v_v/u_{cv}$, $\cos\theta = w_v/u_{cv}$, where $u_{cv}^2 = v_v^2 + w_v^2$ and

$$\frac{\partial u_\theta}{\partial x} = \frac{\partial u_\theta}{\partial r}(-\tan\varphi_v) \tag{7}$$

Based on this relation between the axial and radial velocity gradients, an estimate of the necessary axial spacing follows:

$$\Delta x = \Delta r/\tan\varphi_v \tag{8}$$

This leads to the definition of the vortex-convection skewness (VCS) parameter η_v:

$$\eta_v = (\Delta x/\Delta r)\tan\varphi_v = A_R\tan\varphi_v \tag{9}$$

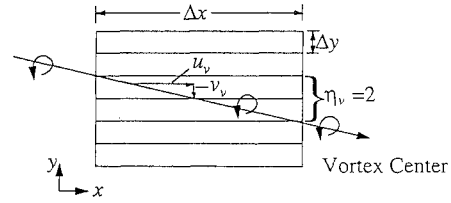

Fig. 4 Diagram of the VCS parameter, $\eta_v = u_{cv}\Delta x/u_v\Delta r$.

Note that Δr should be taken as $2^{1/2}\Delta y$, since this is the maximum grid spacing across the vortex when using a uniform Cartesian mesh. The preceding argument is heuristic and was borne out by numerical experiment.

Based on the estimate of Eq. (9), the vortex-convection skewness (VCS) parameter η_v must be near 1.0 to provide accuracy in the axial direction consistent with the crossflow resolution. If $\eta_v > 1$, the axial grid spacing will be the primary contributor to the numerical diffusion. Note that this is a very restrictive limitation even for small skew angles. For the worse case, when $\tan\varphi_v = 1.0$, Δx must be the same as Δr. This is intuitive since, for this case, there will be no distinction between the crossflow and axial directions. For small skew angles, such as that for a helicopter tip vortex in hover ($\tan\varphi_v \approx 0.13$ on a cylindrical grid due to the wake contraction), the grid aspect ratio must be 8. Considering how fine the crossflow spacing must be to resolve the vortex and the length of the axial direction ($x = 250$), an A_R of 8 would require many grid points.

The meaning of η_v is shown schematically in Fig. 4 (for $z = z_c$, thus $y = r$). A value of $\eta_v = 2.0$ is used just as an example and doesn't correspond to any of the cases run. The VCS parameter represents the number of grid cells the vortex crosses in the crossflow direction for every grid cell of travel in the axial direction.

Boundary Conditions

At the upstream boundary of the model problem, the flow was described by the analytical definitions of the Rankine and Lamb–Oseen vortices. Typical subsonic inflow and outflow boundary conditions were used based on the characteristic flow quantities. For the inlet boundary, total pressure, total temperature, and flow angle were fixed by the analytic vortex definitions and the outgoing Riemann invariant was extrapolated from the interior domain. For the exit boundary, all flow variables were extrapolated, and then the static pressure was adjusted to have a specified area-averaged pressure value, consistent with given upstream total pressure. For the far-field (side) boundaries, the faces corresponding to the maximum distance from the vortex center, the velocities were extrapolated and the total temperature and total pressure were held fixed to the values computed at the upstream boundary. The axial convection Mach number was 0.4, and the peak crossflow Mach number of the vortex was taken as 0.1.

For the double-vortex model problem, two corotating vortices were specified at the upstream boundary. The velocities were combined by linear superposition, and the flow angles were then specified. This initial condition works well as long as the two vortices are not too close together. The vortex centers were separated by a distance of 12 at the upstream boundary.

Computational Grid

The basic grid used for this study was constructed algebraically. The grid was Cartesian in the vicinity of the vortex with uniform grid spacing. Figure 5 shows the entire grid in the crossflow (y–z) plane. The normalized width of the uniform Cartesian grid is 4×4. The vortex core size can grow by a factor of 2 and still be within the uniform grid region. All vortices in this study remained within the uniform grid region.

Outside of the uniform Cartesian grid, the grid was stretched rapidly to the far field where it becomes circular at a radius of 80. For the baseline grid, there were 21 points in the axial direction and 47×47 grid points in the crossflow plane. This included about 7×7 points within the vortex and 21×21 points in the uniform Cartesian grid. Several other grid densities were also used.

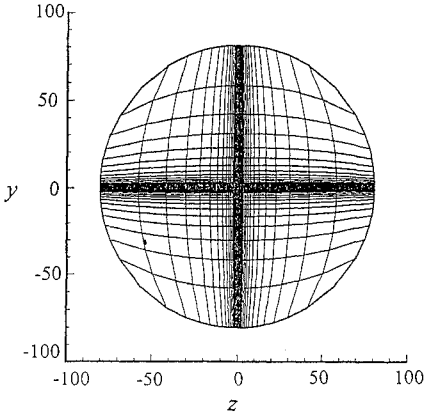

Fig. 5 Complete view of the crossflow grid with 47 × 47 points.

Three different axial convection lengths were examined in the single-vortex study: 8, 80, and 800. After discounting the extrapolation to the upstream and downstream boundaries, the actual convection distances of the vortex computed by the solver were 7.2, 72, and 720. The short and medium length domains were used to perform parametric studies with the solver. In general, as a final test, the long domains were used. For a helicopter blade or fixed wing, the vortex core radius is nominally one-tenth of the chord. Based on this nominal value, these cases were representative of 0.72, 7.2, and 72.0 chord lengths of travel. The medium length grid is typical of a downstream boundary of a computational fluid dynamics (CFD) wing calculation. The long case represents almost one rotor revolution of travel for a helicopter tip vortex.

For the double-vortex model problem, the region of the uniform mesh was large enough to include the two vortices and their rotation as they convect downstream. This requires significantly more grid points than the single vortex case. To have 11 points across the core diameter of each vortex, 91 × 91 points were needed in each crossflow plane.

Results

The calculations, for the most part, were for the inviscid Euler equations. The reason for solving the Euler equations is that the correct inviscid solution is known, that is, zero diffusion of the initial vortex. Any diffusion of the computed vortex would be numerical, due to the truncation error that depends on the grid spacing and the order of accuracy. For this problem, generally, the numerical diffusion of the inviscid terms overwhelms the viscous diffusion. Most of the calculations were performed on a SGI Indigo II workstation with the R4400 processor. Using single precision for the 21 × 47 × 47 grid, the time per iteration was 5.4 s for second-order accuracy and 5.9 s for fifth-order accuracy. These times include the computation of the viscous terms and the turbulence model even though they were not used. Some of the larger cases were run on the Cray C-90.

Convergence Characteristics

For most cases, the axial length of the domain was increased by increasing the grid spacing without changing the number of axial grid points. Increasing the number of grid points in the axial direction did not offer an accuracy benefit unless the aspect ratio reached a large enough value. An increase in the aspect ratio of the cells did have some effect on the convergence characteristics of the problem. The convergence characteristics are briefly discussed here to address some of the tradeoff issues when using a higher order scheme.

The convergence histories of the maximum residual for the short cases ($x = 72$) for several orders of accuracy are shown in Fig. 6. The number of iterations required to reach convergence varied from about 475 for second order to about 725 for fifth order, a 50% increase. The higher order calculations take longer to converge because the high-frequency disturbances are not damped out as quickly. The convergence history for the long case ($x = 720$) for several orders of accuracy are shown in Fig. 7. For the long case, the number of iterations to convergence increased by roughly a factor of 10 (about 4000 iterations for second order and 9000 for fifth order). This was primarily due to the increased time required for

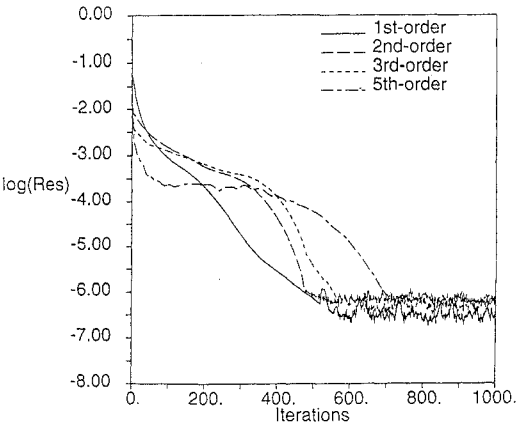

Fig. 6 Residual history for several orders of accuracy, Lamb–Oseen vortex, $x = 72$ case.

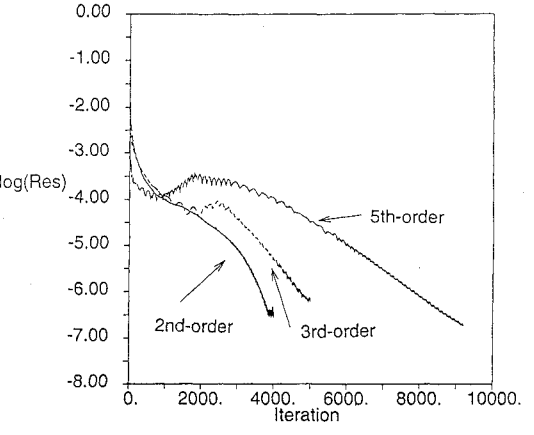

Fig. 7 Residual history for several orders of accuracy, Lamb–Oseen vortex, $x = 720$ case.

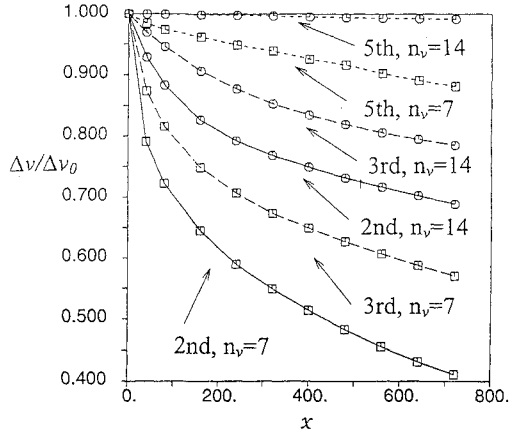

Fig. 8 Computed peak-to-peak velocities vs axial distance for the Lamb–Oseen vortex.

disturbances to travel the length of the domain. The time step was limited by the crossflow spacing, thus the same time step was used even when the length of the domain increased. Once the disturbance reached the end of the domain (at about 2500 iterations for the long case), the residual generally dropped more rapidly. A secondary effect was the increased aspect ratio that had a stronger effect on the higher order schemes. This is believed to be the reason that the fifth-order calculations required more than 10 times the number of iterations for the long case.

Single-Vortex Problem

In Fig. 8 the peak-to-peak vertical velocities across the vortex diameter, normalized by the initial value, are shown vs axial distance. In this figure, the results for several orders of accuracy are shown using 7 and 14 points across the vortex core diameter. Using

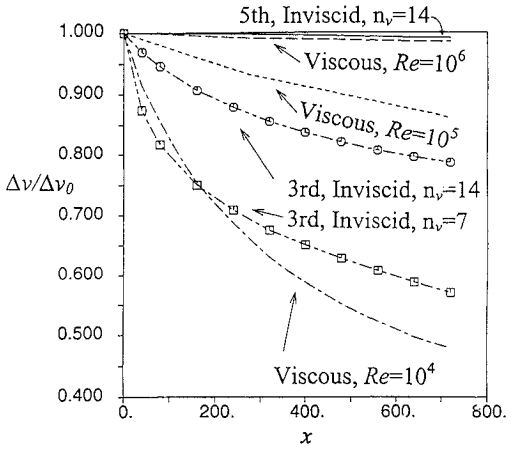

Fig. 9 Computed peak-to-peak velocities vs axial distance for the Lamb–Oseen vortex with viscous effects.

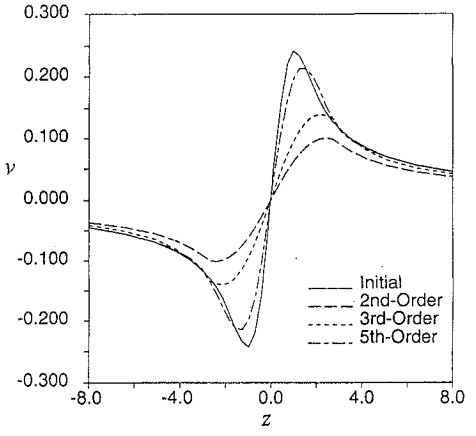

Fig. 10 Computed vertical velocity profiles at x = 720 for the Lamb–Oseen vortex with n_v = 7.

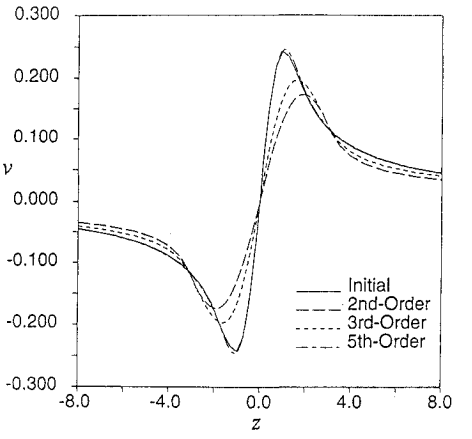

Fig. 11 Computed vertical velocity profiles at x = 720 for the Lamb–Oseen vortex, with n_v = 14.

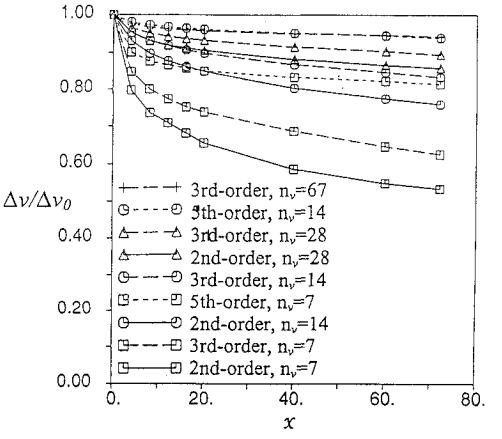

Fig. 12 Predicted peak-to-peak vertical velocities vs axial distance for the Rankine vortex.

second-order accuracy with $n_v = 7$, the peak-to-peak value decayed to 0.41 of its initial value when it traveled a distance of 720. The third-order method provided a significant improvement over second order but still gave poor results ($\Delta v/\Delta v_0 = 0.51$). The fifth-order calculations produced a large improvement and preserved 0.88 of the peak velocities. Using 14 points across the core with third-order accuracy did not do as well as fifth-order with 7 points. Furthermore, the fifth-order predictions with $n_v = 14$ provided excellent vortex preservation ($\Delta v/\Delta v_0 = 0.992$).

Refinement of the crossflow spacing improved the results considerably (error based on the peak-to-peak velocity reduced from 12 to 0.8% for the fifth-order results), but a theoretical convergence rate was not achieved. This is to be expected for several reasons. The grid refinement was performed for the crossflow spacing only, and the axial spacing was not reduced. This increased the cell aspect ratio, which affects the accuracy somewhat, especially for very large aspect ratios (greater than 100). Also, as mentioned previously, the schemes are only formally nth-order accurate for one-dimensional linear problems since the difference stencils are aligned with the grid. Finally, the vortex velocity profile represents a near discontinuity in the flowfield, relative to the other dimensions of the problem and the grid spacing, and this may also cause a deviation from the theoretical convergence rate.

In Fig. 9, the decay of the normalized peak-to-peak velocities are shown for several viscous cases with Reynolds numbers of 10^4, 10^5, and 10^6 (based on the nominal chord). For the viscous calculations, fifth-order differencing was used with $n_v = 14$ to minimize the numerical diffusion. The decay of Δv for the third-order inviscid calculations ($n_v = 7$ and 14) and the fifth-order inviscid case ($n_v = 14$) are also shown in this figure for comparison with the viscous cases. For this problem, the third-order inviscid calculations ($n_v = 7$ and 14) diffused at close to the same rate as the viscous cases with Reynolds numbers of 1×10^4 and 1×10^5. The high Reynolds number case exhibited very little diffusion. The viscous contribution to the diffusion for $Re = 10^6$ was about equal to the numerical diffusion of the fifth-order accurate scheme with $n_v = 14$. The velocity profiles at the downstream boundary for the long case are shown in Figs. 10 and 11 for $n_v = 7$ and 14. For $n_v = 7$, the second-order and third-order results are inadequate, whereas the fifth-order results are good. Using 14 points, the fifth-order results are almost perfect.

Many cases were run for the Rankine vortex, using the medium length domain ($x = 72$). In Fig. 12 are the peak-to-peak velocities vs axial distance for several different orders of accuracy and grid spacing within the vortex core. These comparisons provide an additional indication of the grid refinement needed with lower order methods to achieve the equivalent results of the higher order methods.

For the Rankine vortex calculations, the peak-to-peak values dropped off sharply initially and then approached a linear decay rate. The third-order calculations were refined to 67 points across the core diameter. Although the finest third-order results were similar to the fifth-order results with $n_v = 14$ over this length, the fine third-order results were slightly better since they had a lower decay rate.

This will make a difference for longer cases. Based on these results and those in Fig. 8 for the Lamb–Oseen vortex, the third-order scheme requires nominally 10 times as many points in each crossflow plane to obtain similar accuracy.

Corotating Vortices

Third-order calculations were made for the double-vortex problem using several different grid aspect ratios, defined as $A_R = \Delta x/2^{1/2}\Delta y$, for this simple problem. To describe the skewness of the vortex convection relative to the grid, a VCS parameter, η_v, was derived previously. For the vortex strengths and locations used in this problem, $\tan \varphi_v = 0.04$. Thus η_v will be greater than 1.0 for grid cells with A_R greater than 25.

In Fig. 13, the decay rates of the peak-to-peak velocities are shown for various values of η_v using third-order accuracy and $n_v = 11$ for

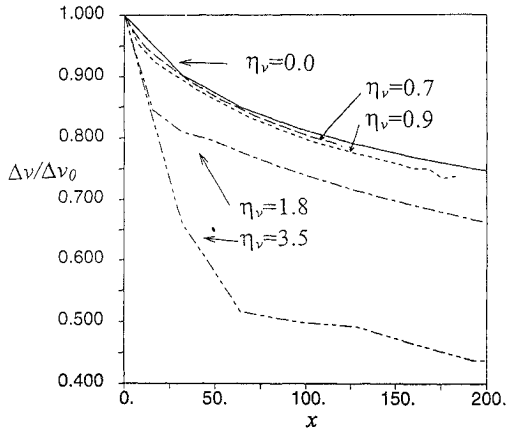

Fig. 13 Predicted peak-to-peak velocities vs axial distance for double-vortex using third-order accuracy.

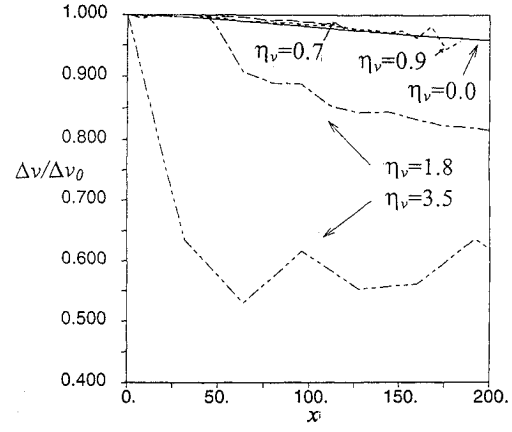

Fig. 14 Predicted peak-to-peak vertical velocities vs axial distance for double-vortex using fifth-order accuracy.

each vortex. For values of η_v less than 1.0, the decay rates of Δv were all about the same. This decay rate was very close to that of the single-vortex case ($\eta_v = 0.0$), also shown in Fig. 13. For the case in which $\eta_v = 1.8$, the vortex diffused rapidly initially and then leveled off to a rate similar to the lower values of η_v. With a VCS level on $\eta_v = 3.5$, the double-vortex structure diffused quickly and combined into one diffused vortex structure after an axial distance of 80. The VCS parameter indicates the axial grid spacing required to achieve an accurate convection of the skewed vortex. In Fig. 14, fifth-order results are shown for the double-vortex case for several values of the VCS parameter. The fifth-order scheme again improved the resolution of the vortex significantly. But the fifth-order scheme exhibited the same sensitivity to the VCS parameter. For a VCS value of 3.5, the double vortex diffused quickly but did not collapse into a single vortex structure until an axial distance of 400. This can be seen by the sharp dropoff in Δv at this location.

Grid Cell Aspect Ratio

Several studies were also performed in which the length of the domain was held constant and the axial spacing was reduced by increasing the number points in the axial direction. Refinement of the grid in the axial direction did not effect the solution when the VCS parameter was less than 1.0. This is consistent with the results of the study presented in Figs. 13 and 14 in which the axial spacing was increased by lengthening the domain. The VCS parameter for the single-vortex problem indicates that the axial spacing and grid cell aspect ratio can be infinite. This, of course, is not true. However, it was found that the axial grid spacing did not begin to affect the results of the single-vortex problem until the grid cell aspect ratio was increased to about 300–400.

Concluding Remarks

An upwind-biased finite volume method with higher order differencing was applied to two model tip-vortex problems. For problems in which the vortex must be maintained over a large distance, this study has shown that it is more efficient to use a higher order scheme rather than to increase the number of grid points with a lower order method. The vortex was preserved almost perfectly over a distance of 72 chord lengths using a fifth-order scheme with 14 points across the vortex core diameter for the well-aligned single-vortex problem. Good preservation was also achieved by using seven points across the core. To achieve this level of accuracy using the third-order method required about three times the number of grid points in each crossflow direction. This will translate to about 10 times the number of grid points in each crossflow plane and 30 times as many points for a three-dimensional grid in the vicinity of a skewed vortex.

This study provides guidelines for the vortex grid spacing required to adequately resolve a vortex over a large distance and indicates that higher orders of accuracy will help in this regard. The axial grid spacing was found to be very important even for small skew angles between the vortex and the grid. A VCS parameter was defined, which indicates the necessary axial spacing required to resolve a vortex that is skewed relative to the grid. This was found to be very limiting in terms of the number of grid points required in the axial direction. For practical applications, the use of higher order schemes and the significance of the VCS parameter need to be investigated further.

Acknowledgments

The authors would like to thank United Technologies Research Center (UTRC) for providing support under the UTRC Fluid Dynamics Core Program. The Numerical Aerodynamic Simulation computer facility was used for some of the larger cases.

References

[1]Srinivasan, G. R., and Baeder, J. D., "TURNS: A Free-Wake Euler/Navier–Stokes Method for Helicopter Rotors," *AIAA Journal*, Vol. 31, No. 5, 1993, pp. 959–961.

[2]Wake, B. E., and Baeder, J. D., "Evaluation of a TURNS Analysis for Hover Performance Prediction," Proceedings of the American Helicopter Society Aeromechanics Specialists Conf., San Francisco, CA, Jan. 1994.

[3]Strawn, R. C., and Barth, T. J., "A Finite-Volume Euler Solver for Computing Rotary-Wing Aerodynamics of Unstructured Meshes," *Proceedings of the 48th Annual American Helicopter Society Forum*, Vol. 1, American Helicopter Society, Washington, DC, 1992, pp. 419–428.

[4]Duque, E.-P. N., "A Structured/Unstructured Embedded Grid Solver for Helicopter Rotor Flows," *Proceedings of the 50th Annual American Helicopter Society Forum*, Vol. 2, American Helicopter Society, Washington, DC, 1994, pp.1249–1258.

[5]Hariharan, N., and Sankar, L. N., "Higher-Order Numerical Simulation of Rotor Flow Field," *Proceedings of the 50th Annual American Helicopter Society Forum*, Vol. 2, American Helicopter Society, Washington, DC, 1992, pp. 1275–1286.

[6]Dacles-Mariani, J., Rogers, S., Kwak, D., Zilliac, G., and Chow, J., "A Computational Study of Wing-Tip Vortex Flowfield," AIAA Paper 93-3010, July 1993.

[7]Choi, D., "A Navier–Stokes Analysis of Film Cooling in a Turbine Blade," AIAA Paper 93-0158, Jan. 1993.

[8]Choi, D., "Three-Dimensional Navier–Stokes Analysis for a Tip Leakage Flow in a Low Aspect Ratio Turbine," AIAA Paper 92-0395, Jan. 1992.

[9]Choi, D., and Knight, C. J., "Application of Scalar Implicit Approximate Factorization for an Underwater Magneto Hydrodynamic Propulsion System Analysis," *AIAA Journal*, Vol. 31, No. 2, 1993, pp. 286–293.

[10]Choi, D., Weeratunga, S., and Knight, C. J., "A Numerical Method for Navier–Stokes Equations with Finite Rate Chemistry," AIAA Paper 98-1857, June 1989.

[11]Roe, P. L., "Approximate Riemann Solvers, Parameter Vectors, and Difference Scheme," *Journal of Computational Physics*, Vol. 43, No. 2, 1981, pp. 357–372.

[12]Roberts, T. W., "Euler Equation Computations for the Flow Over a Hovering Helicopter Rotor," Ph.D. Dissertation, Dept. of Aeronautics and Astronautics, Massachusetts Inst. of Technology, Cambridge, MA, Nov. 1986.

[13]Mounts, J. S., and Barber, T. J., "Numerical Analysis of Shock-Induced Separation Alleviation Using Vortex Generators," AIAA Paper 92-0751, Jan. 1992.

[14]Sreedhar, M. K., and Ragab, S. A., "Large Eddy Simulation of a Longitudinal Vortex," AIAA Paper 94-0529, Jan. 1994.

[15]Batchelor, G. K., *An Introduction to Fluid Dynamics*, Cambridge Univ. Press, New York, 1967.